Inorganic Chemistry

Article

pubs.acs.org/IC

Excited State Properties of Diiron Dithiolate Hydrides: Implications in the Unsensitized Photocatalysis of H_2 Evolution

Luca Bertini, Piercarlo Fantucci, Luca De Gioia, and Giuseppe Zampella*

Department of Biotechnology and Biosciences, Università degli Studi di Milano-Bicocca, Piazza della Scienza 2, 20126 Milan, Italy

Supporting Information

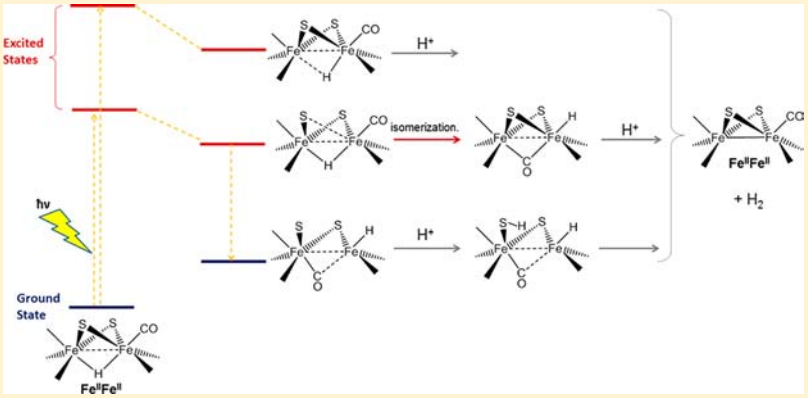

ABSTRACT: Density functional theory (DFT) and time-dependent DFT (TDDFT) have been used to investigate how visible light photons can excite an asymmetrically substituted diiron hydride, $[Fe_2(pdt)(\mu\text{-}H)(CO)_4dppv]^+$ ($\mathbf{1}^+$, dppv = *cis*-1,2-$C_2H_2(PPh_2)_2$; pdt = 1,3-propanedithiolate), as well as the symmetric species $[Fe_2(pdt)(\mu\text{-}H)(CO)_4(PMe_3)_2]^+$ ($\mathbf{2}^+$), which are the first photocatalysts of proton reduction operating without employing sensitizers (Wang, W.; Rauchfuss, T. B.; Bertini, L.; Zampella, G.; *J. Am. Chem. Soc.*, **2012**, *134*, 4525). Theoretical results illustrate that the peculiar reactivity associated to the excited states of $\mathbf{1}^+$ and $\mathbf{2}^+$ is compatible with three different scenarios: (i) it can arise from the movement of the hydride ligand from fully bridging to semibridging/terminal coordination, which is expected to be more reactive toward protons; (ii) reactivity could be related to cleavage of a Fe−S bond, which implies formation of a transient Fe penta-coordinate species that would trigger a facile turnstile hydride isomerization, if lifetime excitation is long enough; (iii) also in line with a Fe−S bond cleavage is the possibility that after excited state decay, a highly basic S center is protonated so that a species simultaneously containing $S-H^{\delta+}$ and $Fe-H^{\delta-}$ moieties is formed and, once reduced by a suitable electron donor, it can readily afford H_2 plus an unprotonated form of the FeFe complex. This last possibility is consistent with ^{31}P NMR and IR solution data. All the three possibilities are compatible with the capability of $\mathbf{1}^+$ and $\mathbf{2}^+$ to perform photocatalysis of hydrogen evolving reaction (HER) without sensitizer. Moreover, even though it turned out difficult to discriminate among the three scenarios, especially because of the lack of experimental excitation lifetimes, it is worth underscoring that all of the three pathways represent a novelty regarding diiron carbonyl photoreactivity, which is usually associated with CO loss. Results provide also a rationale to the experimental observations which showed that the simultaneous presence of donor ligands (dppv in the case of $\mathbf{1}^+$) and a H ligand in the coordination environment of diiron complexes is a key factor to prevent CO photodissociation and catalyze HER. Finally, the comparison of photoexcitation behavior of $\mathbf{1}^+$ and $\mathbf{2}^+$ allows a sort of generalization about the functioning of such hydride species.

INTRODUCTION

Solar energy conversion, that is, the idea of converting the renewable energy source par excellence into chemical energy is a crucial step to overcome the dependence on fossil fuels. In this context, H_2 evolution from light-driven H_2O splitting can be considered the cleanest and convenient solar energy conversion process for large-scale H_2 production.

A homogeneous photocatalytic system for H_2 production typically consists of a sensitizer, an electron donor, and a catalyst, usually based on earth scarce noble metals such as second- and third-row transition metals. In this research area, many efforts have been put to develop systems based on first-row transition metals, as in the case of hydrogenases bioinspired systems. Indeed, in the past 10 years numerous studies on photoinduced H_2 production have been reported[1−3] in which a model of the [FeFe]-hydrogenases active site is coupled with a photosensitizer to form a molecular dyad[4−9] (if the model and the photosensitizer are covalently linked) or a two-component system.[10−12] In both cases, such units have been successively coupled with an electron donor and a proton

Received: April 3, 2013
Published: August 16, 2013

   dx.doi.org/10.1021/ic400818t | *Inorg. Chem.* 2013, 52, 9826−9841

source for light-driven H_2 evolution with encouraging turnover number and photostability.

Recently, a novel route for photoinduced H_2 production has been reported[13] in which the diiron hydrides $[Fe_2(pdt)(\mu\text{-}H)Fe(CO)_4dppv]^+$ ($\mathbf{1}^+$, Scheme 1) was used as *unsensitized* photocatalyst of H_2 production:

Scheme 1. Pictorial Structure of the Complex $[Fe_2(pdt)(\mu\text{-}H)(CO)_4(dppv)]^+$ ($\mathbf{1}^+$)

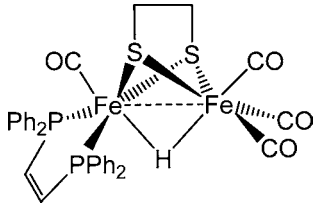

$$[(\mu\text{-}H)Fe_2(pdt)(CO)_4(dppv)]^+ + H^+ \xrightarrow{h\nu} [Fe_2(pdt)(CO)_4(dppv)]^{2+} + H_2$$

In such a photodriven reaction, complex $\mathbf{1}^+$ yields H_2 when irradiated with visible light from a Hg lamp using a λ = 400 nm cut-filter. The dicationic product is very electron poor (formally containing only 32 valence electrons), has a low stability, and tends to degrade, possibly through CO dissociation. To prevent catalyst decomposition, a ferrocene-based electron donor can be used to restore the initial complex $\mathbf{1}^+$, thus closing the catalytic cycle. The complex $[(\mu\text{-}H)Fe_2(pdt)(CO)_4(PMe_3)_2]^+$ ($\mathbf{2}^+$), which has been the subject of several experimental and computational studies,[14,15] behaves similarly. From a photochemical standpoint, it is noteworthy that $\mathbf{1}^+$ and $\mathbf{2}^+$ are coordinatively saturated and, upon irradiation, ligand dissociation might occur, in agreement with the general photochemical behavior of transition metal carbonyl complexes[16] and in particular with the recent findings regarding CO photolysis of the simple Fe^IFe^I $Fe_2(pdt)(CO)_6$ complex.[17−21]

Protonated Fe^IFe^I complex features photochemical properties which were previously unknown and that likely involve high energy excited states. Previous density functional theory (DFT) and time-dependent DFT (TDDFT) calculations carried out studying a very simplified model of $\mathbf{1}^+$, in which phenyl groups were substituted with hydrogen atoms, did not reveal significant changes in the electronic structure upon irradiation,[13] even though a less symmetric arrangement of the Fe-μH-Fe portion of the molecule was evident in some excited states. Concomitantly, it was shown that an isomer of $\mathbf{1}^+$ featuring terminal-axial hydride coordination is very unstable if compared to the bridging hydride at the ground state level, but the energy gap between the two isomers decreases at the excited state level. Both observations suggested a similar consequence: light energy could provide the hydride system with more "terminal-like" hydride character. Actually, either the breaking of symmetry of the bridging coordination of the hydride to the two Fe ions or alternatively, easier formation of the terminally coordinated hydride, might be associated with the higher reactivity toward protonation, since fully symmetric Fe−H−Fe hydrides show poor or no reactivity toward acids, at least according to kinetics reports on some members of this class of compounds.[22,23] In fact, a DFT study has recently rationalized the greater reactivity toward acids of terminally coordinated hydrides in terms of frontier-orbital arguments.[24] It must be underscored, however, that the reactivity of terminally bound hydrides in diiron compounds is strictly dependent on the oxidation state and/or on the properties of the coordination set: some *bis*-diphosphine complexes (such as $[(terminal\text{-}H)Fe_2(pdt)(CO)_2(dppv)_2]^+$) still need to undergo one-electron reduction for reacting with protons and releasing H_2, whereas more basic *bis*-diphosphine derivatives (such as the $[(terminal\text{-}H)Fe_2(edt)(CO)_2(PMe_3)_4]^+$) directly yield H_2.[20,21] Thus, independently of the source, it is evident that electrons residing in higher occupied MOs have to be endowed with the proper energy to observe H_2 generation by such diiron hydrides. The necessary energy may derive from light, which could excite electrons to high energy levels. This last observation is in line with the reported unsensitized photoreactivity of $\mathbf{1}^+$ and $\mathbf{2}^+$, which lack both of the necessary basic properties (only two P ligands) and also of the more suitable ($Fe^{II}Fe^I$) reduction level. Indeed, it has been shown experimentally that additional electron donors are needed to make $\mathbf{1}^+$ a hydrogen evolving reaction (HER) catalyst in a strict sense. In a similar scenario, it cannot be excluded that part of the photon energy can be employed to activate fast unimolecular processes such as photoisomerization leading from μ-hydride to more reactive species. In light of the recent results on the photochemistry of $Fe_2(pdt)(CO)_4(PMe_3)_2$,[25] such photoisomerization might be assisted by weakening or dissociation of Fe-ligand bonds.

Prompted by previous results, we aimed to investigate by DFT and TDDFT the photochemistry of $\mathbf{1}^+$ and $\mathbf{2}^+$,[13] starting from a general analysis of the electronic structure of protonated Fe^IFe^I models. Herein we have modeled explicitly all the phenyl groups of dppv, but, to avoid complications due to the propanedithiolate (pdt) flipping, the ethanedithiolate bidentate ligand (edt) has been adopted in place of pdt. Nevertheless, we will refer to edt and pdt derivatives as $\mathbf{1}^+$ (or $\mathbf{2}^+$) indistinguishably to avoid further complication throughout the discussion. Moreover, we explored all relevant portions of the excited state potential energy surfaces (PES) which are likely involved in photochemistry experiments, by focusing onto those aspects closely related to ligand dissociations and H_2 production. Further, with the aim of exploring one of the possible roles played by photon energy in generating hydrides activated toward protonation, we provide computational evidence about the greater thermodynamic and kinetic accessibility of the photoisomerization process "unreactive/μ-H→reactive/terminal-H" over that resulting from the ground state analogue. Finally, we stress that the primary objective of the present contribution was not the investigation of the global mechanism of the photo-HER process, but rather to inspect whether photon energy can promote formation of species with higher protonation propensity. As it will be shown, such species feature weakened Fe-L bonds, where L = H and S.

■ COMPUTATIONAL DETAILS

Computations were performed using the pure Generalized Gradient Approximation (GGA) BP86 DFT functional[26,27] and the Resolution of Identity[28] (RI) technique, as implemented in the TURBOMOLE[29] suite of programs. Basis sets of triple-ζ plus polarization split valence quality (def2-TZVP hereafter)[30] were adopted for all atoms in the complexes. The DFT grid-size was set to standard m3 value. Analytical gradients for the TDDFT excited state energy were computed using the EGRAD routine recently implemented[31] within TURBOMOLE in combination with the RI.[32]

dx.doi.org/10.1021/ic400818t | Inorg. Chem. 2013, 52, 9826−9841

Excited PESs have been scanned along selected Fe-Ligand (Fe-L) bond stretching coordinates as follows. For each step, the ground state structure was first optimized by keeping the elongated Fe-L distance fixed. Finally, the first 15 TDDFT excitations were computed on the ground state relaxed structure. The Fe-L distances were stretched until complete ligand dissociation. The sampling of the excited PES has been carried out with a step of 0.05 Å until the energy difference between two consecutive steps on the ground state PES was less than 1×10^{-5} hartree.

Transition states occurring along the pathway of isomerization have been located by means of an efficient quasi-Newton−Raphson algorithm, in which the preliminary step is the structure optimization of a guess of the putative transition structure. In such optimization, all those degrees of freedom composing the reaction coordinate and which are therefore expected to change most during the reaction occurrence, must be kept frozen. Subsequently, the analytical Hessian calculation of the energy minimized point reveals the proximity to the first-order saddle point on the PES, by showing the presence of an imaginary frequency associated with the reaction coordinate normal mode. Such mode is then unfrozen and exploited in an eigenvector following procedure, in which the direction information deriving from an approximated Hessian is exploited by means of the so-called updating techniques of the Hessian matrix itself. If the starting point is not significantly distant from the desired stationary point (a first order saddle, in the case of transition state structures) convergence is reached within a few steps of the algorithm run, as typical of *trust radius* (i.e., a region of confidence where a local quadratic approximation to the PES is accurate) based methods of optimizations.

RESULTS AND DISCUSSION

General Features of the Electronic Structure of Protonated Fe^IFe^I Models. The electronic structure of the diiron core of several $[Fe^IFe^I]$-hydrogenase synthetic models has been the subject of several studies. It is well established that the highest occupied molecular orbital (HOMO) and the lowest unoccupied molecular orbital (LUMO) of such complexes[33] are essentially characterized by Fe−Fe σ-bonding and σ*-antibonding combination of the Fe d_{z^2} atomic orbitals. Focusing on the bridging hydride formed upon protonation of Fe^IFe^I species, the interaction between the s orbital of the incoming proton with the HOMO and LUMO of a generic Fe^IFe^I model is shown in Scheme 2.

The hydride species is characterized by the Fe-μH-Fe three-center two-electron bond with a doubly occupied MO that originates from the interaction between the HOMO of the parent model with the hydrogen orbital. The interaction with the LUMO results in the formation of an unoccupied MO which is nonbonding with respect to one of the two Fe-μH bonds. These two MOs formed upon H^+ binding are not necessarily the HOMO and the LUMO of the μ-protonated form. In particular, the Fe-μH-Fe bonding MO could be lower in energy with respect to the HOMO, because of the favorable orbital interaction between hydrogen s and Fe d_{z^2} orbitals. Finally, there is a second unoccupied MO which turns out to be antibonding or nonbonding with respect to both Fe-μH bonds and is thus expected to be higher in energy. Therefore, according to the qualitative MO diagram (Scheme 2), some of the low-lying excited states of a protonated Fe^IFe^I model could feature monoelectronic transitions resulting in population of an antibonding or nonbonding Fe-μH MO, depending on the energy of the MOs involved. In such case, the migration of the Fe-μH bonding electron density would entail the weakening of at least one Fe-μH bond, possibly making the hydride more reactive toward subsequent protonation. The possibility of observing a low-lying charge transfer (CT) excitation toward a hydride based orbital can be excluded because such an unoccupied MO is too high in energy.

Scheme 2. Schematic Representation of the Interaction between the s Orbital of the Incoming Proton and the HOMO and LUMO of a Fe^IFe^I Dithiolate, Also Corresponding to the Core of the Active Site of [FeFe]-Hydrogenase

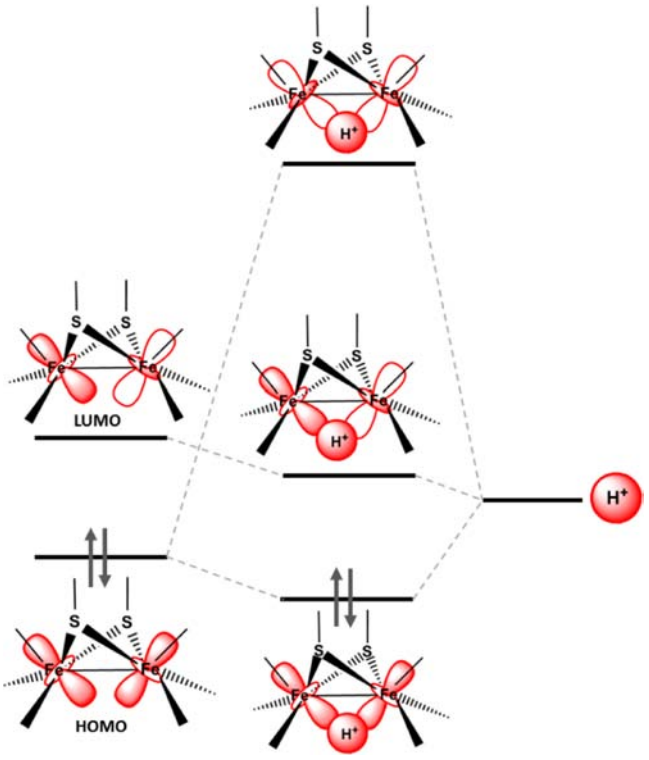

The photoinduced reactivity of Fe-μH-Fe species could be due to the formation of a terminal hydride isomer generated upon excitation. This possibility was evaluated comparing the electronic structure of the unprotonated Fe^IFe^I rotated structure (i.e., the structure in which one CO ligand occupies a bridging position, which is actually a transition state structure) and of its corresponding terminal protonated form. Upon rotation of one of the two FeL_3 moieties in the unprotonated form, the shape of the HOMO significantly changes and is characterized by a lobe of density that occupies the vacant axial position on the rotated Fe atom.[34] The interaction between the HOMO of the rotated species with the incoming H^+ generates a low energy bonding Fe−H MO (HOMO-20) in the terminal hydride form. The LUMO of the unprotonated form is bonding with respect to the Fe-bridging CO interaction involving the rotated Fe atom. Analogously to the HOMO, the lobe of the orbital in the LUMO also spans the apical site of the rotated Fe and forms a bonding interaction with H, as shown in Scheme 3.[22]

This observation implies that when the LUMO of the protonated form is populated upon excitation, the terminal hydride might result stabilized with respect to the bridging hydride.

TDDFT Spectrum. The computation of the electronic spectrum of the species under investigation is a prerequisite to any discussion of a photochemical process. The experimental UV−vis spectrum of $[Fe_2(pdt)(\mu\text{-H})(CO)_4(dppv)]^+$ $(\mathbf{1}^+)$[13] has three prominent features: (i) a low intensity band at 500 nm

dx.doi.org/10.1021/ic400818t | Inorg. Chem. 2013, 52, 9826−9841

Scheme 3. Schematic Representation of the Interaction between the s Orbital of an Incoming Proton and the HOMO and LUMO of a Rotated $Fe^{I}Fe^{I}$ Form

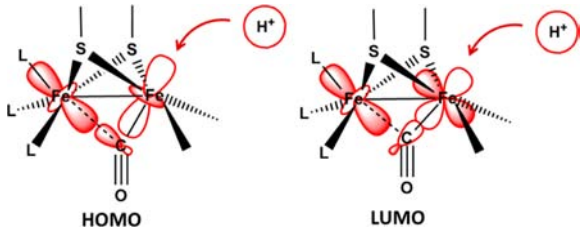

with a shoulder at 575 nm; (ii) a more intense shoulder at 380 nm; (iii) an intense band around 300 nm. The corresponding TDDFT spectrum of $\mathbf{1}^{+}$ is reported in Figure 1.

A total of 30 singlet excited states and their corresponding oscillator strength and main monoelectronic transitions were computed (Table 1). The computed spectrum features four low-intensity bands in the region between 557 and 437 nm, and two intense bands at 425 and 360 nm, with the corresponding excitations involving the MOs in the range HOMO-5/LUMO +2. The nature of these excitations can be discussed on the basis of the orbital composition of the frontier MOs. In Table 2 the Mulliken MO populations are reported for MOs in the range HOMO-7/LUMO+2.

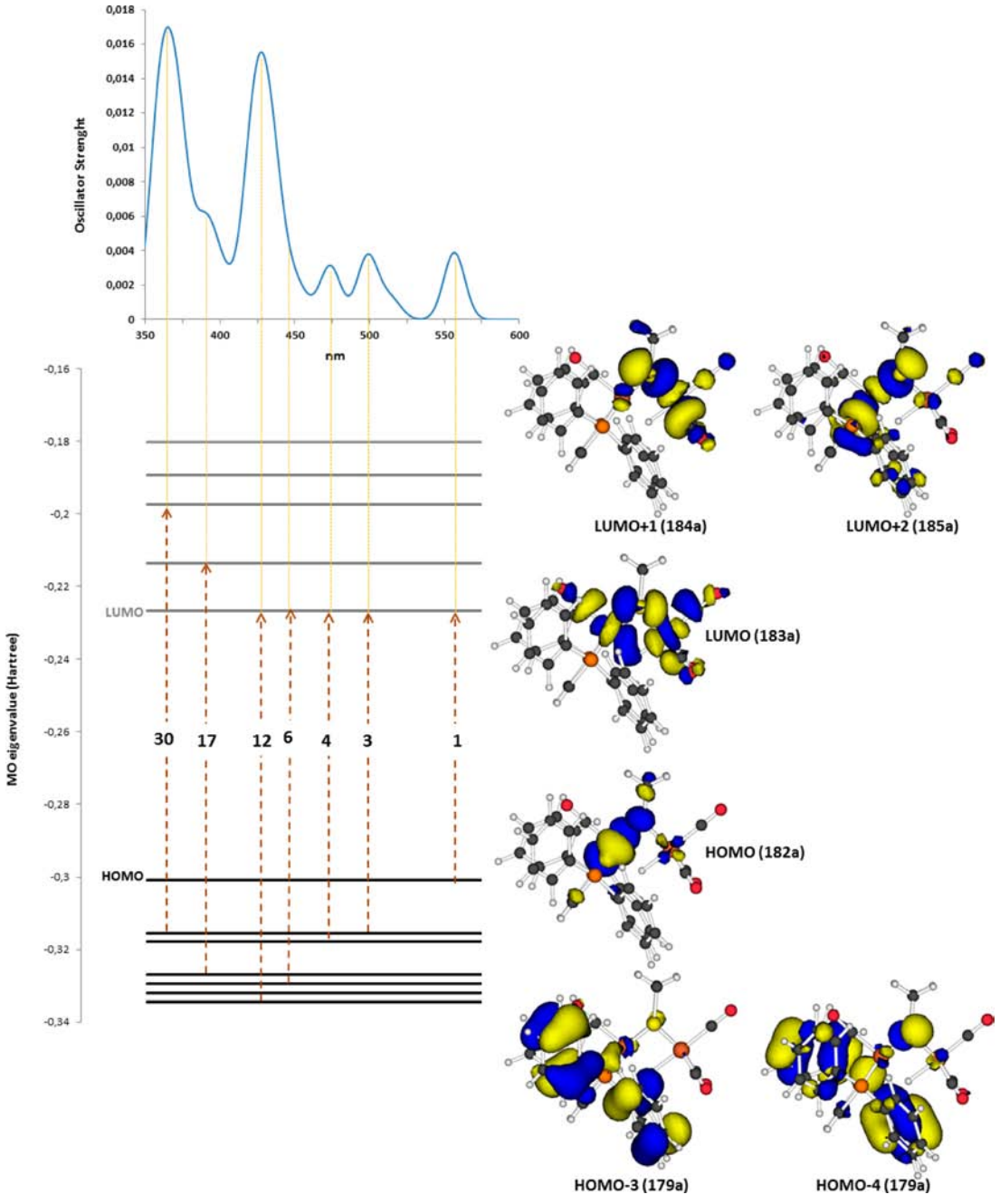

Figure 1. TDDFT spectrum of $\mathbf{1}^{+}$ and band assignment according to the computed main one-electron transitions (see Table 1). Isosurface plots of the frontier MOs computed at 0.05 au.

dx.doi.org/10.1021/ic400818t | Inorg. Chem. 2013, 52, 9826−9841

Table 1. TDDFT Electronic Spectrum of 1^{+a}

excitation	nm	f	1e
1	556.7	3.9×10^{-3}	182a→183a (97.4)
2	514.3	1.1×10^{-3}	182a→184a (97.2)
3	498.8	3.7×10^{-3}	181a→183a (96.9)
4	473.6	3.1×10^{-3}	180a→183a (96.4)
5	452.3	1.6×10^{-3}	179a→183a (97.2)
6	441.2	1.7×10^{-3}	178a→183a (95.8)
7	436.5	3.3×10^{-3}	182a→185a (97.4)
8	432.8	4.4×10^{-4}	177a→183a (99.0)
9	430.4	5.7×10^{-3}	181a→184a (74.5)
			180a→184a (19.6)
10	428.0	2.2×10^{-3}	180a→184a (76.1)
			181a→184a (18.5)
11	423.7	2.6×10^{-3}	176a→183a (78.5)
			175a→183a (20.1)
12	420.9	4.6×10^{-3}	175a→183a (75.8)
			176a→183a (17.6)
17	399.0	2.0×10^{-3}	179a→184a (90.8)
30	359.1	7.6×10^{-3}	181a→185a (29.7)
			180a→185a (28.6)
			181a→186a (17.3)

[a]For each transition are reported the excitation energy (nm), the oscillation strength (f), and the main monoelectronic excitations (1e) with the corresponding percentage composition. The band assignments are made on the basis of the transition which has the closest excitation energy with respect to the maximum of each band of the computed spectra.

In general, the contributions of sulfur atomic orbitals in the unoccupied MOs are always larger than in occupied MOs. Importantly, this observation implies that all excitations involve charge transfer toward the sulfur atoms. The MOs from HOMO-2 to HOMO are essentially Fe based MOs with a dominant contribution from the atomic orbitals of the Fe ion chelated by dppv (designed as Fe_{dppv}). This is reminiscent of a previous work by Borg et al.[35] and Heinekey et al.[36] on the reduction of $Fe_2(SR)_2$ compounds. In the LUMO/LUMO+2 MOs, the Fe orbital contributions decrease in favor of contributions from ligand based orbitals. Particularly relevant is the increase of edt contributions (mainly localized on sulfur atoms) and the dppv contribution for LUMO+2. It is also noteworthy that the LUMO has similar contributions from both Fe atoms. In particular, the LUMO is characterized by Fe-μH bonding orbital combinations on the dppv side, whereas it is nonbonding with respect to the other Fe-μH bond. Finally, HOMO-3/HOMO-7 are essentially π-phenyl localized MOs. The fully bonding orbital, centered on the Fe-μH-Fe core (i.e., MO no. 161, HOMO-20) lies much lower in energy compared to the HOMO.

The assignment of each excitation can be made on the basis of the monoelectronic transitions (Table 1), which have been computed by TDDFT, and the corresponding MO populations (Table 2). The differential MO populations for each excited state (ex; Table 3) are calculated as follows

$$\Delta q_{ex} = \sum_n (q_{i,n} - q_{a,n}) c_n$$

where $q_{i,n}$ and $q_{a,n}$ are the atomic populations for the i unoccupied and a occupied MOs involved in the $a \rightarrow i$ monoelectronic transitions with weight equal to c_n.

In general, all excited states (Table 3) are associated with charge transfer (CT) to S atoms of the edt ligand. The first four excited states (S1−S4) originate from population of the LUMO in which both Fe atoms are equally populated and display significant $Fe_{dppv} \rightarrow Fe_{(CO)3}$ MMCT and $Fe_{dppv} \rightarrow$(S,CO) MLCT character. The S5, S6, S8, S11, and S12 states feature a dppv→Fe LMCT character and display a significant π density migration from the dppv phenyl rings to the Fe atoms. These excited states could play an important role in the photochemistry of the system at 400 nm, according to the band assignment proposed above. Such finding underlines also the necessity of using a full representation of the chelate structure to obtain a correct picture of the electronic structure of reactivity-related orbitals.

Exploration of the Excited State PES. The interest in investigating the properties of the excited states of $\mathbf{1}^+$ arises directly from the experimental observation that this complex can perform HER *without any sensitizer*. Also, to address the photostability of $\mathbf{1}^+$ related to CO loss (typical of non-

Table 2. Atomic and Group Mulliken MO Populations of the Ground State of 1^+

	175	176	177	178	179	180	181	182	183	184	185
	HOMO-7	HOMO-6	HOMO-5	HOMO-4	HOMO-3	HOMO-2	HOMO-1	HOMO	LUMO	LUMO+1	LUMO+2
Fe_{dppv}	0.049	0.056	0.011	0.084	0.085	1.267	1.415	1.554	0.563	0.08	0.79
$Fe_{(CO)3}$	0.012	0.011	0.006	0.042	0.02	0.183	0.12	0.062	0.581	0.812	0.07
ΣFe	0.061	0.067	0.017	0.126	0.105	1.45	1.535	1.616	1.144	0.892	0.86
Edt	0.054	0.02	0.003	0.178	0.19	0.103	0.057	0.174	0.353	0.629	0.426
CO dppv	0.025	0.027	0.004	0.018	0.021	0.159	0.22	0.005	0.126	0	0.011
CO trans	0	0	0	0.008	0.006	0.022	0.017	0.006	0.056	0.155	0.019
	0.004	0	0	0.002	0.004	0.028	0.015	0.003	0.057	0.173	0.02
CO apical	0	0	0	0.004	0.005	0.003	0	0.01	0.136	0.057	0.054
dppv	1.832	1.863	1.955	1.626	1.639	0.203	0.146	0.23	0.116	0.073	0.591
ΣP	0.046	0.028	0.016	0.095	0.108	0.072	0.018	0.101	0.063	0.035	0.301
ethylen	0.015	0.023	0.009	0.029	0.031	0.021	0.001	0.027	0	0.003	0.011
$(Ph)_4$	1.771	1.812	1.93	1.502	1.5	0.11	0.127	0.102	0.053	0.035	0.279
μH	0.002	0.002	0	0.001	0	0.008	0	0	0.02	0	0

dx.doi.org/10.1021/ic400818t | Inorg. Chem. 2013, 52, 9826−9841

Table 3. Differential Mulliken MO Populations Computed According to the TDDFT Main One-Electron Excitations

	S1	S2	S3	S4	S5	S6	S7	S8	S9	S10	S11	S12	S17
Fe_{dppv}	−0.248	−0.368	−0.213	−0.175	0.120	0.120	−0.190	0.138	−0.308	−0.285	0.128	0.128	−0.003
$Fe_{(CO)3}$	0.130	0.188	0.115	0.100	0.140	0.135	0.003	0.145	0.160	0.150	0.143	0.143	0.198
ΣFe	−0.118	−0.180	−0.098	−0.078	0.260	0.255	−0.190	0.283	−0.148	−0.135	0.270	0.270	0.198
Edt	0.045	0.115	0.075	0.063	0.040	0.045	0.063	0.088	0.133	0.125	0.080	0.078	0.110
CO dppv	0.030	−0.003	−0.023	−0.008	0.028	0.028	0.003	0.030	−0.050	−0.040	0.025	0.025	−0.005
CO trans	0.013	0.038	0.010	0.008	0.013	0.013	0.003	0.015	0.033	0.033	0.015	0.015	0.038
	0.013	0.043	0.010	0.008	0.013	0.015	0.005	0.015	0.038	0.035	0.015	0.013	0.043
CO apical	0.033	0.013	0.035	0.033	0.033	0.033	0.010	0.035	0.013	0.013	0.035	0.035	0.013
dppv	−0.028	−0.040	−0.008	−0.023	−0.380	−0.378	0.090	−0.460	−0.020	−0.028	−0.435	−0.430	−0.393
ΣP	−0.010	−0.018	0.013	−0.003	−0.013	−0.008	0.050	0.013	0.003	−0.005	0.008	0.005	−0.018
ethylen	−0.008	−0.005	0.000	−0.005	−0.008	−0.008	−0.005	−0.003	0.000	−0.003	−0.005	−0.005	−0.008
$(Ph)_4$	−0.013	−0.018	−0.018	−0.015	−0.363	−0.363	0.045	−0.470	−0.020	−0.018	−0.438	−0.433	−0.368
μH	0.005	0.000	0.005	0.003	0.005	0.005	0.000	0.005	0.000	−0.003	0.005	0.005	0.000

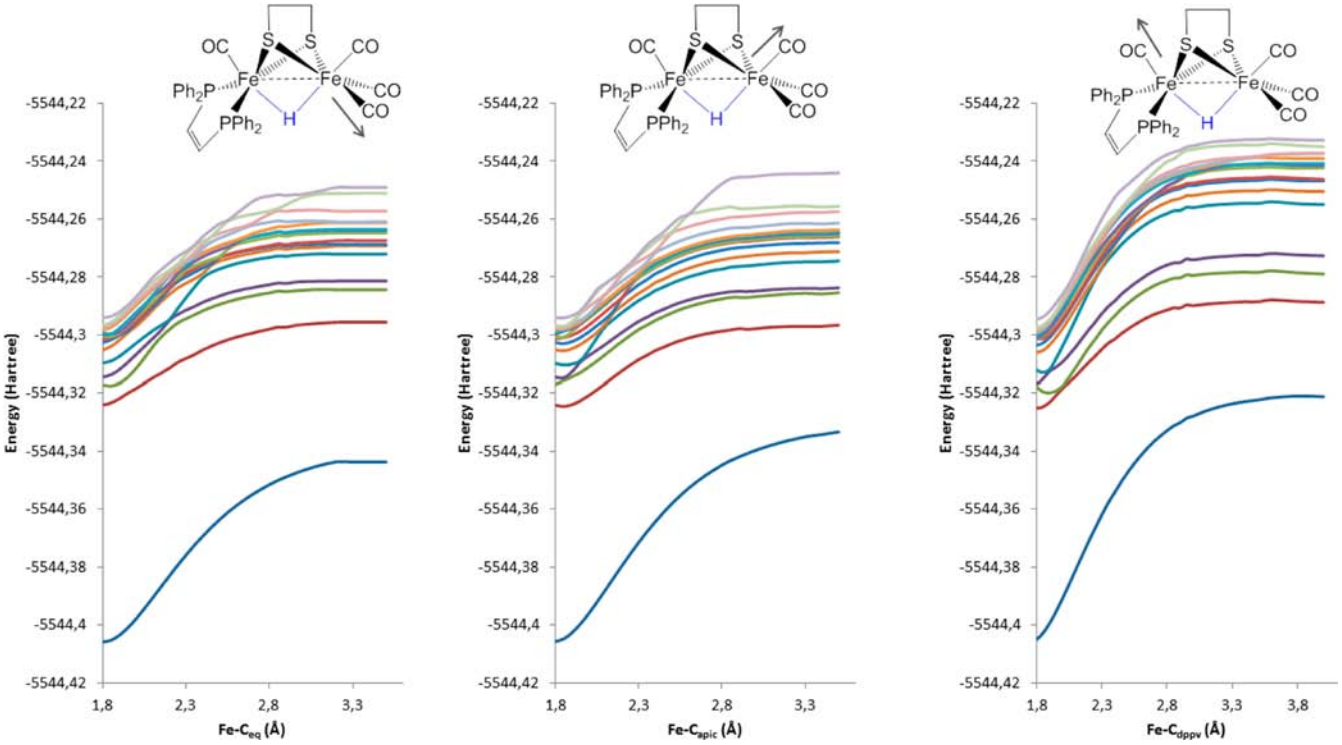

Figure 2. PES of the 1^+ ground state and of the first 15 excited states along the following coordinates: Fe−C_{eq} (left), Fe−C_{apic} (middle), and Fe−C_{dppv} (right). The stretched bond is indicated by an arrow in each molecular sketch.

substituted diiron carbonyls) we have characterized the excited states related to CO photodissociation, by exploring the excited state PES along the three possible Fe-CO stretching coordinates (both apical and equatorial CO of $Fe(CO)_3$ side and apical CO of Fe(CO)dppv side) starting from the ground state geometry. The scans of the singlet excited PES are reported in Figure 2.

All excited state PESs result essentially bound with respect to CO dissociation, even if energy barriers result always lower with respect to the corresponding values computed on the ground state PES (on average −16.1 kcal·mol^{-1} equatorial; −23.1 kcal·mol^{-1} apical; −19.2 kcal·mol^{-1} dppv side).[37] The lowest energy barrier is found for S4 along the apical coordinate (16.2 kcal·mol^{-1}). Equatorial and apical CO photodissociations from the $Fe(CO)_3$ moiety are favored with respect to CO dissociation on the dppv side, likely because of the decrease of the hydride bridging character concomitant to the dppv Fe−C bond dissociation. Results are in line with the observed photostability and the IR features indicating stronger Fe-CO bonds in 1^+ (and in general in disubstituted $Fe_2L_2(CO)_4$ derivatives) compared to that of less basic all-carbonyl analogues.[17]

Subsequently, we have explored the excited state PES topology along the Fe-μH-Fe→Fe···μH-Fe, Fe−S, and Fe−P stretching modes. Along the first mode, the hydride partially loses its bridging character, an observation that is particularly relevant to identify on which excited PES a semibridging

dx.doi.org/10.1021/ic400818t | Inorg. Chem. 2013, 52, 9826−9841

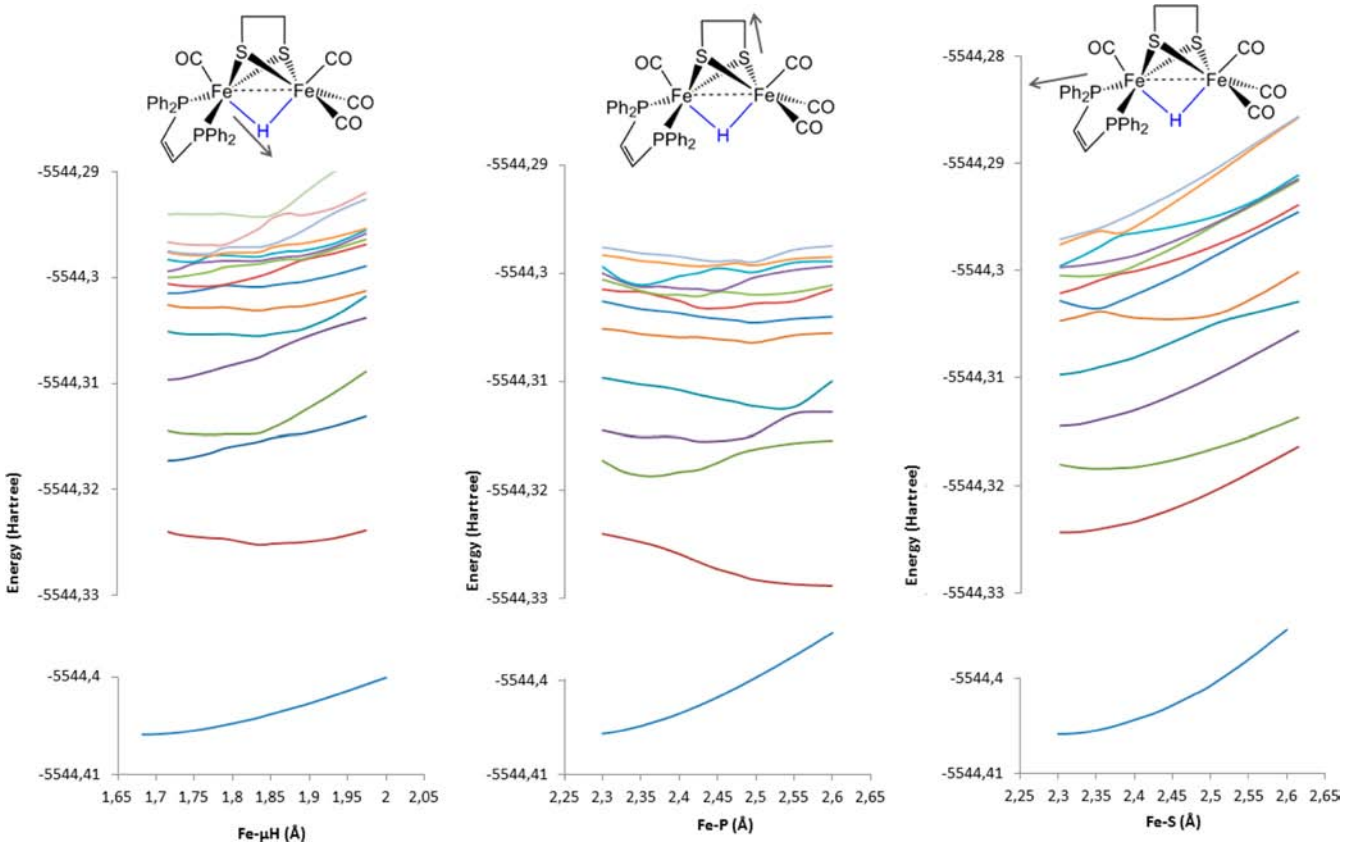

Figure 3. PES of the 1^+ ground state and the first 15 excited states along the Fe-μH-Fe→Fe···μH-Fe, Fe−S, and Fe−P bond stretching coordinates. The stretched bond is indicated by an arrow in each molecular sketch.

hydride coordination is stabilized. Indeed, the initial step of the hydride photoactivation may consist in the partial destabilization of the bridging coordination toward a semibridging/terminal coordination. The second and third stretching are considered to evaluate possible effects of either dppv or edt detachment from Fe.

In Figure 3 the PES scans are reported along the (i) Fe-μH-Fe→Fe···μH-Fe stretching coordinate, in the Fe-μH distance range between the ground state value (1.682 Å) to 2.0 Å with a step of 0.025 Å; (ii) Fe−S and Fe−P stretching modes (2.3 to 2.6 Å, step of 0.025 Å).

Concerning the Fe-μH stretching scan, for most of the excited states considered, the total energy decreases going toward a semibridging hydride coordination, at least as long as the longer Fe-μH distance is 1.85 Å. For longer values, structure distortion becomes significant, and the total energy increases. Moreover, most of the excited PESs are quite flat and relatively insensitive to variations of Fe-μH distances. In contrast, the ground state PES is far more sensitive to changes in Fe-μH distances. This observation highlights the stabilization gained by the semibridging hydride coordination on the excited state PES.

Along the Fe−S stretching mode, the energy state S1 has a clear dissociative character, with a total energy decrease of 3.0 kcal·mol^{-1} computed comparing the ground state and the 2.6 Å Fe−S stretched optimized structure (Fe−S bond distances in the ground state minimum structure are 2.263 and 2.299 Å). Also S4 has the same feature of S1, but undergoes a state crossing with S3 around 2.55 Å. Finally, along the Fe−P stretching scan, lower energy states are bound, while S6 features a state crossing with S5 that successively undergoes energy decrease until 2.5 Å. Therefore, TDDFT results suggest that upon light irradiation 1^+ could undergo Fe−S bond cleavage and/or loss of the bridging coordination of the hydride, while both CO loss and Fe−P bond cleavage are unlikely events.

TDDFT Geometry Optimizations. As the next step in the investigation of the initial stages associated with 1^+ irradiation we have carried out TDDFT geometry optimizations using the ground state structure as starting point, to understand the excitation effect of each state on hydride coordination and on Fe-L bond distances.[38] The main structural parameters for the first 12 excited states are reported in Table 4. Before analyzing such results, it must be pointed out that only S1 and S3 converged to stationary points. When convergence criteria were not met, the parameters associated with structures featuring the lowest energy/gradient norm vector are reported. For S7 and S11, the main monoelectronic excitations indicate a state crossing with the S6 and S10 states, respectively.

Some general trends are evident in the variations of the geometry parameters. The $\Delta\mu$ values (defined as the difference between the longest and the shortest Fe-μH distances), as well as the Fe−Fe and Fe−S bond distance elongations for the optimized excited state structures are reported in Figure 4. Compared to the ground state structure, for all the excited states considered (i) the Fe−Fe and Fe−S distances result always elongated; (ii) the Fe−P distances show less significant variations and the Fe−C−O bond angle is slightly bent in a few states (S1 and S3); (iii) the bridging hydride character decreases.

Regarding the optimized structure for S1, we found a marked elongation (0.422 Å) of one Fe−S bond (Fe(CO)$_3$ side). This result nicely confirms the Fe−S dissociative character already

dx.doi.org/10.1021/ic400818t | Inorg. Chem. 2013, 52, 9826−9841

Table 4. TDDFT Optimized Geometry Parameters (Distances in Å, Angles in Degrees)[a]

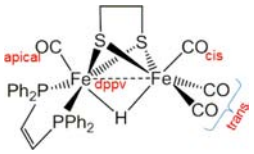

				Fe–S		Fe–H				Fe–C			
										apical		equatorial	
	1e	conv	Fe–Fe	prox	dist	prox	dist	Δμ	Fe–P	dist	angle	dist	angle
GS			2.615	2.263	2.299	1.703	1.683	0.02	2.263	1.750		1.804	
										1.791			
S1	H→L	yes	2.662	2.322	2.721	1.648	1.732	0.084	2.331	1.769		1.828	168.4
					2.284					1.772		1.785	
S2	H→L+1 (64.9)	no	2.685	2.325	2.402	1.648	1.742	0.094	2.297	1.839		1.797	172.5
	H→L (33.1)				2.412					1.807		1.811	
S3	H-1→L (66.2)	yes	2.698	2.330	2.384	1.634	1.742	0.108	2.297	1.839	173.5	1.806	
	H→L+1(32.9)									1.803		1.802	
S4	H-2→L (59.4)	no	2.732	2.344	2.373	1.644	1.712	0.068	2.294	1.835		1.803	175.6
	H-1→L (37.9)									1.811			
S5	H→L+2	no	2.740	2.314	2.373	1.638	1.760	0.122	2.255	1.800		1.795	
S6	H-5→L	no	2.790	2.315	2.334	1.614	1.846	0.232	2.222	1.830	171.2	1.781	
										1.791			
S7	→S6												
S8	H-7→L (65.3)	no	2.754	2.313	2.360	1.625	1.802	0.177	2.232	1.780	174.6	1.789	
	H-5→L (30.4)									1.814			
S9	H-5→L (53.1)	no	2.697	2.320	2.411	1.654	1.727	0.073	2.260	1.800		1.800	173.8
	H-4→L (42.7)				2.386							1.805	
S10	H-8→L	no	2.767	2.310	2.352	1.625	1.811	0.186	2.231	1.803		1.788	
S11	→S10												
S12	H-1→L+1 (82.2)	no	2.706	2.322	2.393	1.650	1.733	0.083	2.254	1.800		1.800	
	H-1→L+1 (14.9)												

[a]Prox and dist refer to the Fe atom that brings the dppv ligand (prox) and that brings the three CO ligands (dist); Apical and equatorial CO ligands are defined with respect to the brigding hydride; Δμ is the difference between the longer and the shorter Fe–H distance. Whenever the geometry optimization did not converge to a stationary point ("no" in the conv column) the geometry parameters are reported for the lowest energy/lowest gradient structure obtained during the same optimization calculation.

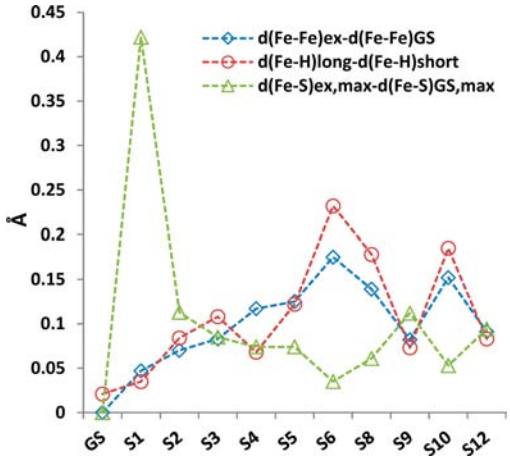

Figure 4. 1^+ Excited state vs ground state optimized geometry parameter comparisons: Fe–Fe, Fe-μH (long)-Fe-μH (short) and Fe–S. All values in Å. The Fe–S values are computed comparing the highest values among the four Fe–S optimized distances for the ground state and the excited states. The labels "ex" and "GS" are used to distinguish between excited states and ground state.

evidenced during the S1 scan along the Fe–S bond elongation coordinate. The differential Mulliken MO populations, coupled to the TDDFT main one-electron excitations for S1, S6, S8, and S10 singlet states, computed at the excited state minimized geometry are collected in Table 5.

The comparison of the two MOs involved in the monoelectronic excitation (the HOMO and the LUMO) highlights a strong Fe→S CT from Fe_{dppv} to the dissociated sulfur atom, which becomes more electron-rich. Such results are consistent with two limit scenarios: (i) the transient five-coordination of the Fe ion, generated upon S ligand detachment/weakening, could favor a rearrangement of the hydride from bridging to terminal position; (ii) alternatively, after excited state decay, S protonation could occur on a high energy isomer of 1^+ in which the S–Fe bond is cleaved. This would imply formation of a diprotonated form, bearing concomitantly $SH^{\delta+}$ and $FeH^{\delta-}$ moieties. More details about both such scenarios will be presented in the next sections.

In the ground state structure of 1^+ the hydride is fully bridged, and Δμ is only 0.021 Å. The highest Δμ (0.233 Å) is found in S6, with the longer Fe-μH bond distance significantly elongated (1.846 Å) compared to the ground state (1.613 Å). Loss of bridging character (Δμ > 0.15 Å) is also found in the S8 and S10 states. It is worth recalling that the symmetry breaking of the Fe–H–Fe moiety was found to be negligible when using a simplified modeling of the dppv ligand,[13] indicating that the full representation of the molecular structure is critical. It is also

dx.doi.org/10.1021/ic400818t | Inorg. Chem. 2013, 52, 9826–9841

Table 5. Differential Mulliken MO Populations Coupled to the TDDFT Main One-Electron Excitations for S1, S6, S8, and S10 1^+ Singlet States Computed at the Excited State Minimized Geometry

	S1	S6	S8	S10
1e	H→L	H-5→L	H-7→L	H-8→L
Fe_{dppv}	−0.365	0.093	0.102	0.110
$Fe_{(CO)3}$	0.203	0.163	0.161	0.170
ΣFe	−0.163	0.256	0.262	0.280
edt	0.172	0.076	0.075	0.077
CO ap	0.047	0.066	0.061	0.069
CO eq	0.138	0.031	0.033	0.034
dppv	−0.057	−0.437	−0.438	−0.467
ΣP	−0.044	0.000	0.000	0.003
ethylen	−0.007	−0.004	−0.004	−0.003
$(Ph)_4$	−0.006	−0.433	−0.435	−0.467
μH	0.010	0.009	0.008	0.009

relevant to note that $\Delta\mu$ nicely correlates with the Fe−Fe bond distance elongation, as shown in Figure 4.

S6, S8, and S10 excitations show a dppv→Fe LMCT and dppv→(CO,S) LLCT character (Table 5). As previously noted, HOMO-5, HOMO-7, and HOMO-8 are essentially π-orbitals of the phenyl rings of the dppv. As expected, population of the σ^* Fe−Fe and Fe-μH antibonding LUMO induces an elongation of the Fe−Fe bond and a weakening of the Fe-μH bond, which are both very evident when the electron density comes from the dppv ligand. Thus, the initial hypothesis[13] concerning the presence of some excited states featuring more terminal hydride character, is corroborated by TDDFT.

Regarding the elongation of the Fe−S bond found in S1, it has to be remarked that such result is correlated to the presence of the bridging hydride. Indeed, TDDFT optimization of the nonprotonated **1** complex (i.e., $[Fe_2(pdt)(CO)_4dppv]$, data not shown) do not show any significant Fe-L bond elongation or any particular distortion of the structure, except Fe−Fe bond elongation. Such results clarify the importance of protonated diiron derivatives in the photo-HER systems. Therefore, the simultaneous adoption of disubstitution and protonation of the prototypical diiron hexacarbonyl propane-dithiolate for photo-HER, which has proven to be successful experimentally, has now a theoretical basis. While the unsubstituted complex is photolabile, the diphosphine substitution makes the Fe-CO bonds stronger. Nonetheless, disubstituted diiron derivatives are reduced at too negative potentials and thus protonation was originally devised to have more favorable reduction potentials (even less negative than those of many sensitizers). Present DFT calculations indicate that a subtle balance exists between seemingly opposite effects: electron donor substitution along with protonation of diiron dithiolates is successful because it entails a different Fe-L labilization than that typically observed in diiron carbonyls, that is, the Fe-CO bond. How the Fe−S and Fe−H elongations can be related to HER is the subject of the following sections.

Ground State vs Lowest Triplet State PES Topology. Photoisomerization of μ-Hydride to More Reactive Isomers (Terminally Coordinated Hydrides). In the preceding section, we have shown that the excited states likely involved in the photochemistry of $\mathbf{1}^+$ are characterized by monoelectronic transitions in which the LUMO becomes populated. The exploration of the corresponding excited state PES using TDDFT geometry optimization suggests that the effects observed when the LUMO becomes occupied upon excitation are (i) partial loss of the bridging character of the hydride; (ii) Fe−S bond elogantion. Regarding the Fe-L bond elongation, results suggest that hydride isomerization might be favored by the partial and transient decrease of the Fe coordination number. To characterize a reaction pathway on a given PES, normal-mode frequencies should be computed to characterize a structure as a local minimum or a transition state. However, it is presently impossible to study a reaction pathway on an excited PES using TDDFT, because energy second derivatives cannot be computed. An approximate strategy to investigate such issue and, more generally, the effects of the LUMO population on photochemistry, implies the computation of the lowest triplet state at the DFT level (the so-called ΔSCF approach). Imposing the triplet single occupation of the HOMO and LUMO, we investigated the lowest triplet state PES (that corresponds to the S1 singlet PES) at the DFT level instead of the TDDFT. This approach allows to use DFT geometry optimizations and vibrational frequency computations, thus permitting to identify and characterize transition state structures. Recently, ΔSCF has been used to show that for $Fe_2(pdt)(CO)_6$, the free energy barriers for the CO dissociation on the triplet PES are almost halved compared to the ground state PES.[39] However, by using such approach only the HOMO→LUMO triplet state can be investigated, since the

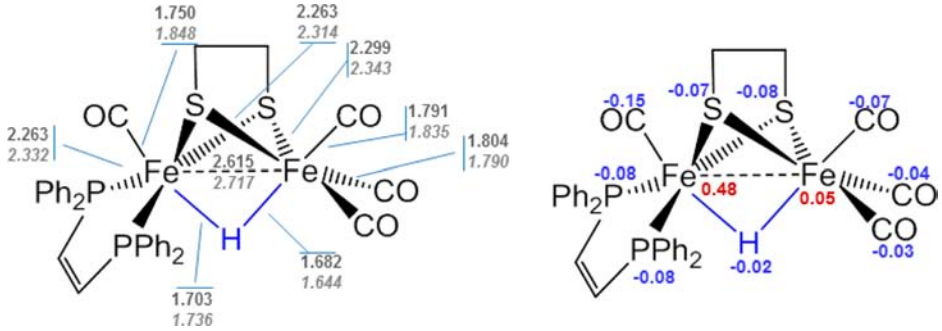

Figure 5. Left: ground state (normal) and lowest triplet state (italics) optimized bond distances (in Å); Right: Atomic or group natural bond order (NBO) charge differences between triplet and ground state. Negative (blue) and positive (red) values indicate an increases or a depletion of electron density, respectively. The value for a molecular ligand is the sum of the atomic NBO charges of the atoms that belong to the ligand.

dx.doi.org/10.1021/ic400818t | Inorg. Chem. 2013, 52, 9826−9841

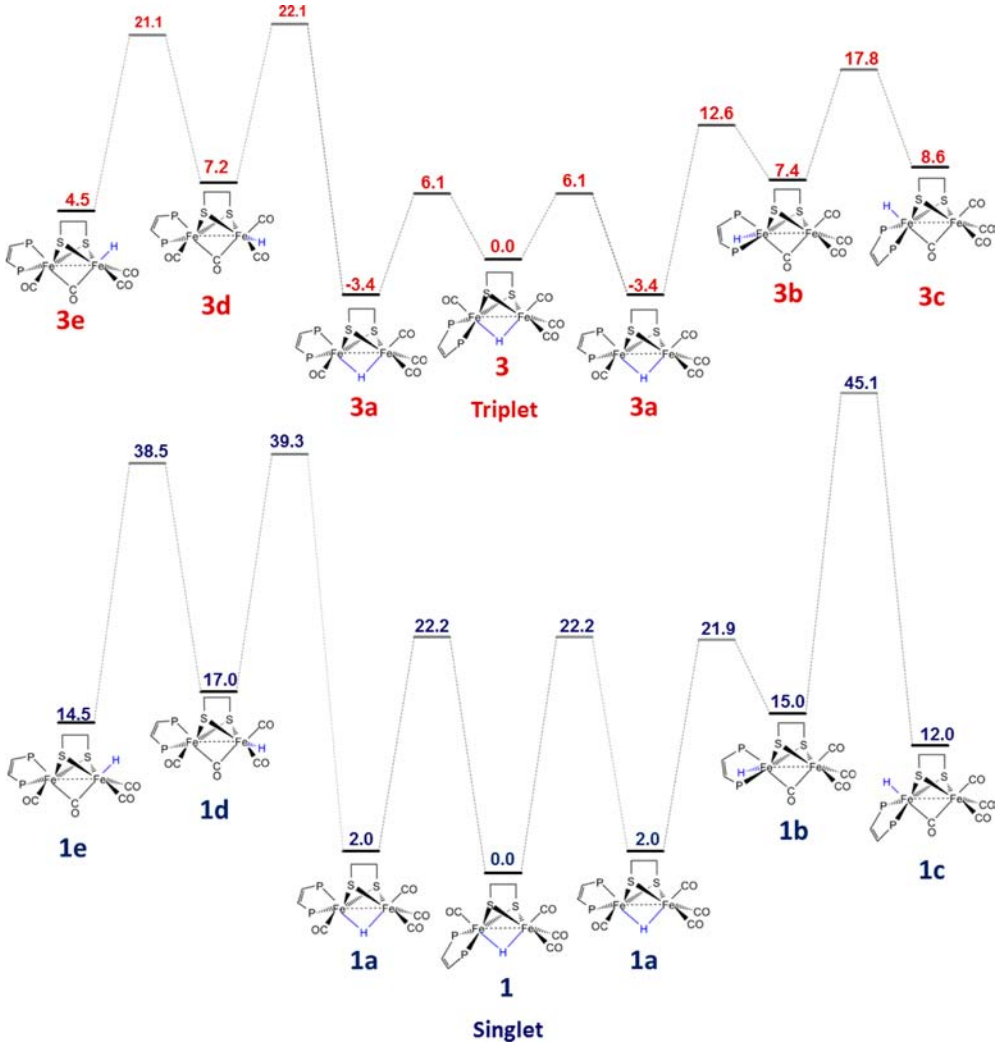

Figure 6. Ground state (bottom/blue) and triplet state (top/red) pathways associated to the isomerization of μ-H (**1** for the singlet pathway; **3** for the triplet pathway) to both possible terminal-axial-H isomers (**1c** and **1e** for the singlet; **3c** and **3e** for the triplet).

system has no molecular symmetry to be exploited to constrain the MO occupation to a different excited state. Although in principle we cannot exclude that this triplet state could be populated (for example via intersystem crossing), in this context we consider this state as a general model for all the excited states likely involved in the photochemical process, which are characterized by a main monoelectronic transition toward the LUMO. In this particular case, the detailed topology of the triplet PES along the bridging-to-terminal hydride reaction pathway can give us a broader view of the photochemical process with respect to the more local TDDFT picture, allowing us to better understand how the population of the LUMO could influence the fluxionality and the reactivity of the system.

The lowest triplet state has HOMO(α)LUMO(α) MO occupation. Compared with the ground state, in the triplet optimized structure, all Fe-X distances result elongated (Figure 5, left; Fe−Fe 0.102 Å, apical Fe−C 0.098 Å and 0.044 Å, equatorial Fe−C 0.014 Å, Fe−P 0.069 Å, Fe−S 0.046 Å on average) and $\Delta\mu$ slightly increases (+0.071 Å). These nuclear distortions are mainly due to the Fe_{dppv}→ligand CT, evidenced by the NBO charge differences (Figure 5; right side).

Another step in the exploration of the triplet PES is the determination of the bridging-to-terminal hydride isomerization pathway, with the aim of verifying if the photoisomerization process is energetically favored compared to the ground state PES. Of course, in the absence of precise lifetime data about the persistence of excited states, it cannot be stated rigorously that nuclear rearrangement processes have time to occur before excitation decay. However, the comparison between thermodynamic and kinetic features associated with ground state and excited state energy profiles might yet provide interesting general hints on photoactivated unimolecular isomerizations processes.

As pointed out previously, on the triplet state PES the terminal hydride isomer is relatively stabilized compared to the bridging isomer with respect to the situation observed on the ground state PES. Besides, also the kinetics of the bridging to terminal hydride rearrangement might differ significantly on the singlet and the triplet surfaces. That could imply that a possible role of the light energy is to speed up the unimolecular process turning the unreactive (or poorly reactive) bridging hydride into a terminal hydride, which is expected to be the most reactive isomer toward protonation.

The ground state terminal-to-μ hydride isomerization pathway in $\mathbf{1}^+$ has been previously studied, but only considering the *term*−H-Fe$(CO)_3$ isomer.[40] When focusing on the terminal-to-bridging direction, such choice is motivated on

dx.doi.org/10.1021/ic400818t | *Inorg. Chem.* 2013, 52, 9826−9841

the basis of other recent DFT results showing that the distal Fe site (the less substituted) is more accessible by acids kinetically, even though such Fe is thermodynamically the less basic one.[41] Also, experimental evidence show that distal iron is in many cases the exclusive site of protonation at very low temperature[20,42,43,36] although just a 20 K increase of temperature affords terminal protonation at both the single Fe sides.[35,44] Herein we have instead considered the possibility that, in the reverse direction (i.e., from bridging to terminal coordination) the hydride could migrate, in principle, to both Fe sites.

Triplet vs Singlet state μH-to-tH Interconversion. Concisely, the lowest energy pathway consists of two subsequent Ray−Dutt twists (rhombic-C_{2v}-like), leading from the axial terminal-H coordination to the bridging-H isomer, passing through an intermediate in which the hydride is coordinated to Fe in terminal-equatorial position.[33] Also, a Bailar twist-like (trigonal-prism-C_3-like) rearrangement may be necessary to switch from axial−equatorial to diequatorial coordination configurations.[33,45] Generally, when both Ray−Dutt and Bailar twists are plausible, the former mechanism is energetically preferred, at least for hexa-coordinated diiron dithiolate compounds.[33] In fact, experimental data are consistent with such unimolecular rearrangement mechanisms.[20,21,36] The pathways of the μH-to-tH interconversion are shown, for both the singlet (ground) state and the triplet (excited) state, in Figure 6. Alternative routes yielding the isomer featuring the hydride coordinated to the distal iron were also investigated (Figure 7). It is important to stress that, even if we report the full pathway leading from μ-H to the terminal/axial-H for sake of completeness, it is likely that possible nuclear rearrangement processes occurring on the excited PES (provided that lifetimes of the excited states are long enough) terminate at the kinetic product, which is the terminal hydride isomer encountered along the pathway, that is, the equatorially coordinated one (**3b**, figure 6).

For sake of simplicity, we report (Figures 6 and 7) only the full energy profiles associated with the hydride migration from the bridging position (**1** and **3**, Figures 6 and 7) to all possible terminal positions, both basal and apical. For a detailed description of each elementary step forming the whole pathways, the reader should refer to Supporting Information (first section). Herein, we limit ourselves to point out that DFT calculations reported in Figures 6 and 7 indicate **3b** as terminally coordinated species being the most easily accessible (kinetic product). The barrier connecting **3a** and **3b** is only *16 kcal/mol*, indicating a kinetic facile process. Though the axial hydride **3e** turned out to be the most stable thermodynamically, yet it is quite likely that kinetic arguments dominate when reactions occurring on excited states are considered. Generally, our results suggest that, on the excited PES, terminal hydride isomers are relatively stabilized compared to the bridging isomer and also that energy barriers to overcome to observe hydride isomerization are by far lower at the excited state level than without irradiation. All that could indicate that photoactivation could be related to a gain of kinetic and thermodynamic attainability of terminal hydride forms. Nevertheless, even though the differences observed comparing triplet and singlet energy profiles are evident, without the knowledge of the experimental lifetime of the excited state it is impossible to state unequivocally that the system has enough time to undergo photoisomerization.

Protonation of a Species Featuring a Cleaved Fe−S Bond at the Ground State. A third scenario can be also

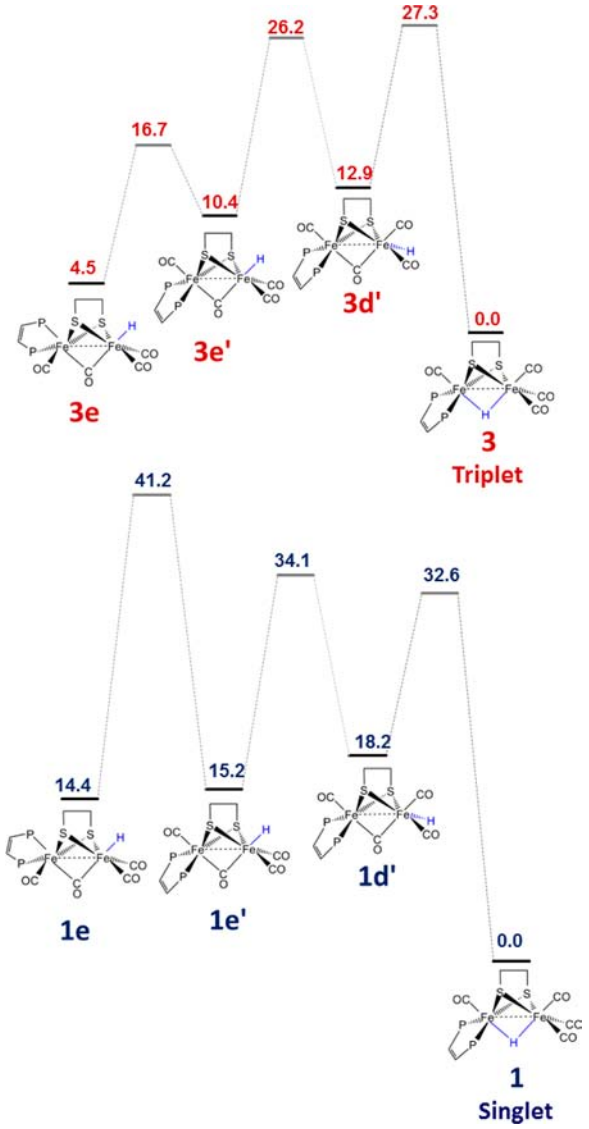

Figure 7. Isomerization pathways alternative to those illustrated in Figure 6. Only the terminal hydrides **1e** and **3e** can be formed by such routes.

envisaged from the TDDFT results presented above. After decay of the excited state associated to the Fe−S weakening/break, namely, S1, a transient and very unstable species can be formed on the ground state PES, which retains an elongated Fe−S bond. Such structure, which has been characterized by DFT ($\mathbf{1}'^{+}$), is less stable than $\mathbf{1}^{+}$ by more than 50 kcal/mol, a value compatible with irradiation in the 400−500 nm range (see Scheme 4). In $\mathbf{1}^{+}$ the hydride ligand loses spontaneously the bridging coordination in favor of a purely terminal one, and the terminal CO on the dppv side moves to a bridging position. This could suggest that Fe−S cleavage and decrease in bridging character of the hydride are somewhat connected. In addition, the S ligand which has lost the bridging coordination is now more basic and is expected to readily protonate in the presence of strong acids (HOTf was used experimentally). Interestingly, the aforementioned structural features of $\mathbf{1}'^{+}$ are reminiscent of super-reduced Fe(I)Fe(0) species, likely involved in electrochemical pathways of dihydrogen production by diiron dithiolates.[46−48] In the light of these observations, three possible protonation/reduction thermodynamic schemes have

dx.doi.org/10.1021/ic400818t | Inorg. Chem. 2013, 52, 9826−9841

Scheme 4. Summarizing Picture of Events Possibly Occurring at the Electronic Ground State after Excitation Decay of a Hydride Species with Elongated (or Even Broken) Fe−S Bond[a]

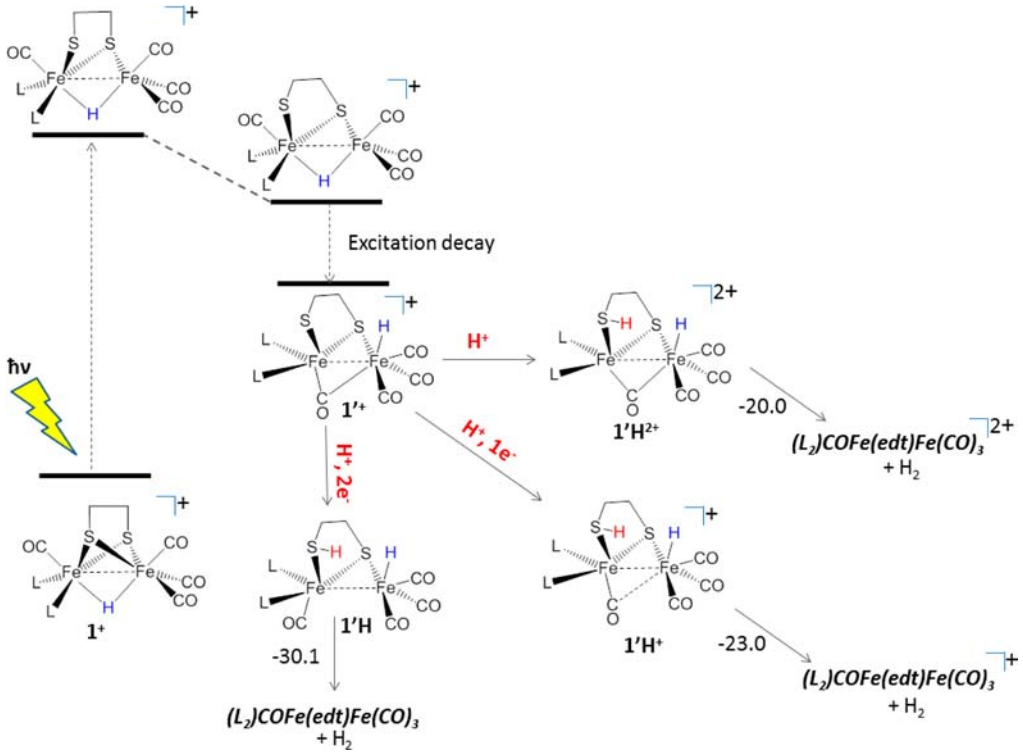

[a]Energetics is shown (only thermodynamics, kcal/mol) associated with catalytic (where reductive step are present) or stoichiometric H_2 production by di-protonated hydride forms.

been considered, corresponding to different experimental conditions: (i) $\mathbf{1'}^{+}$ can be further protonated, if no reducing agent is employed; (ii) $\mathbf{1'}^{+}$ protonation can be coupled to 1e reduction; (iii) $\mathbf{1'}^{+}$ protonation can be coupled to 2e reduction. This last situation is consistent with the experimental detection (^{31}P NMR) of both the unprotonated neutral form **1** and $\mathbf{1}^{+}$ itself.[13] All the three doubly protonated forms, that is, $\mathbf{1'H}^{2+}$, $\mathbf{1'H}^{+}$, and **1′H** (see Scheme 4) share the feature of having simultaneously an acid SH group and a basic hydride (on the $Fe(CO)_3$ moiety), and are therefore expected to readily release H_2. Indeed the HER computed from all of the three structures resulted in a markedly exergonic process. Furthermore, the three structures show a correlation between the reduction level and the extent of CO bridging character: **1′H** has only terminal bound CO ligands, $\mathbf{1'H}^{+}$ has one CO in semibridging position between the two iron ions, and $\mathbf{1'H}^{2+}$ features a fully CO bridged.

Species featuring H_2 coordinated to a single Fe in a η_2 fashion do not correspond to reaction intermediates. In fact, DFT optimization of such structures spontaneously evolve to monohapto coordination modes of the hydride ligands, or to structures in which one hydride is terminally coordinated and the other is in μ-position between the two iron atoms. This could suggest that the mechanism of dihydrogen evolution from the doubly protonated species can be better described as the opposite of a heterolytic H_2 cleavage, rather than as a reductive elimination from a single iron of a Fe−H_2 group.

Subsequently, with the aim of ascertaining some mechanistic details underlying thermodynamic data presented in Scheme 4, reduction potentials have been computed for $\mathbf{1'H}^{2+}$, $\mathbf{1'H}^{+}$, and $\mathbf{1'}^{+}$. For example one could wonder if in the presence of a reducing agent, the species actually releasing H_2 is $\mathbf{1'H}^{+}$ or the more reduced **1′H**. If $\mathbf{1'H}^{+}$ was not reducible at −0.5 V, it could be indicated as the actual H_2 releasing agent. Unfortunately, the comparison of values reported in Table 6

Table 6. Redox Potentials of Some Diiron Dithiolates Presented in Scheme 4[a]

redox couple	redox potential (vs $Fc^{+/0}$ in CH_2Cl_2; V)
$\mathbf{1'H}^{2+/+}$	+0.904 V (calc)
$\mathbf{1'}^{+/0}$	+0.872 V (calc)
$\mathbf{1'H}^{+/0}$	−0.220 V (calc)
$\mathbf{L_2COFe(edt)Fe(CO)_3}^{+/0}$	+0.169 V (calc)
***sym*-(Me_8)-$Fc^{+/0}$**	−0.512 V (exp)
$\mathbf{1}^{+/0}$	−1.39 V (calc); (with pdt, −1.33 V, exp)

[a]Experimental values (exp) are taken from ref 13 (and ref 22 therein).

does not allow such kind of deduction, since, according to DFT, all species in Scheme 4 are potentially reducible at −0.5. As a control, it has been checked if $\mathbf{1}^{+}$ was reducible by sym-Me_8-Fc, to verify whether the reducing agent indeed acted on the dication $[L_2COFe(edt)Fe(CO)_3]^{2+}$, after H_2 release, as indicated in the experimental report,[13] or whether an alternative pathway entailing $\mathbf{1}^{+}$ reduction was followed. In the light of Table 6 data, this latter possibility can be excluded, in that $\mathbf{1}^{+}$ cannot be reduced at −0.5 V.

Characterization of the Excited States of $[Fe_2(edt)(\mu\text{-}H)(CO)_4(PMe_3)_2]^{+}$. The protonated *di*-phosphine derivative $[Fe_2(pdt)(\mu\text{-}H)(CO)_4(PMe_3)_2]^{+}$ has been extensively studied[14] and recently it was shown that also this complex performs photo-HER without sensitizer.[13] Therefore, we carried out the

dx.doi.org/10.1021/ic400818t | Inorg. Chem. 2013, 52, 9826−9841

TDDFT optimization of the low-lying excited state of the $[Fe_2(edt)(\mu\text{-}H)\ (CO)_4(PMe_3)_2]^+$, ($\mathbf{2}^+$) in which the edt has been adopted instead of pdt in line with the investigations carried out on $\mathbf{1}^+$. Analysis of the MOs and excitations for $\mathbf{2}^+$ are collected in the Supporting Information.

Two isomers of the complex $\mathbf{2}^+$ can be defined according to the reciprocal position of the phosphine ligands as $\mathbf{2}^+_{trans-trans}$ and $\mathbf{2}^+_{trans-cis}$ (see Scheme 5),[14,49] where trans and cis refer to the position of the phosphine ligands with respect to the sulfur atoms of the edt ligand.

Scheme 5. Schematic Structure of $\mathbf{2}^+$ Isomers

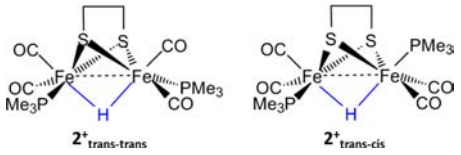

The trans−trans isomer results only 2.9 kcal·mol^{-1} lower in energy compared to the trans−cis form, whereas the cis−cis form in which both PMe_3 ligands occupy the apical position results higher in energy (+6.8 kcal·mol^{-1}) and therefore it will not be considered. The electronic spectra of the two isomers are similar and are reported in the Supporting Information. The first 30 excitations are characterized by monoelectronic transitions that involve MOs in the range HOMO-5/LUMO +2 (the Mulliken MO populations are reported in the Supporting Information). The general features of the MOs of $\mathbf{2}^+$ are similar to those computed for $\mathbf{1}^+$. Fe orbital contributions in the occupied MOs are always higher than those of the unoccupied MOs, while the opposite holds for the sulfur and, to a lesser extent, for the phosphorus orbital contributions. In particular, the overall orbital contributions of the PMe_3 ligands are not as significant as in the case of the phenyl rings of the dppv ligand in $\mathbf{1}^+$ because in the latter case the corresponding MOs lie much higher in energy with respect to the MO localized on the methyl group in PMe_3.

The computed electronic spectra for $\mathbf{2}^+_{trans-trans}$ and $\mathbf{2}^+_{trans-cis}$ were obtained considering the first 20 excitations in the 490 to 300 nm energy range. However, all the important spectral features are in the range 490−360 nm, that corresponds to the first 11 excitations and which is large enough to include all the possible transitions induced by a 400 nm irradiation. The analysis of these excitations using the Mulliken MO differential populations show that almost all excited states in this range are characterized by a Fe→S CT but the Fe contributions change depending of the isomer considered. In the case of $\mathbf{2}^+_{trans-trans}$ both Fe atoms contribute almost equally to the density transfer to the sulfur atoms; in $\mathbf{2}^+_{trans-cis}$ we often observed a positive transfer contribution from the Fe atom that holds the PMe_3 ligand in apical position and, at the same time, a negative

Table 7. $\mathbf{2}^+_{trans-trans}$ TDDFT Optimized Geometry Parameters (Distances in Å, Angles in Degrees)[a]

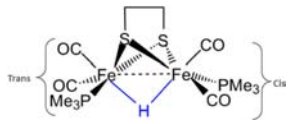

				Fe−S		Fe−H			Fe−P		Fe−C			
	1e	conv	Fe−Fe	trans	cis	trans	cis	Δμ	trans	cis	trans		cis	
GS			2.615	2.290	2.293	1.685	1.684	0.001	2.289	2.288	1.776	1.767	1.7670	1.777
				2.293	2.295									
S1	H→L	yes	2.659	2.308	2.355	1.670	1.698	0.028	2.285	2.305	1.853	1.820	1.773	1.783
				2.347	2.319									
S2	H-1→L	no	2.653	2.332	2.356	1.671	1.673	0.002	2.302	2.305	1.862	1.856	1.775	1.776
				2.354	2.335									
S3	H-2→L (73.9)	no	2.737	2.360	2.362	1.721	1.659	0.062	2.300	2.288	1.850	1.785	1.831	1.777
	H-1→L (21.1)			2.310	2.306									
S4	H-3→L (74.5)	no	2.782	2.303	2.338	1.765	1.652	0.113	2.285	2.301	1.828	1.782	1.836	1.803
	H-1→L (17.2)			2.321	2.326									
S5	H→L+2 (73.4)	no	2.617	2.361	2.325	1.678	1.680	0.002	2.332	2.333	1.796	1.811	1.801	1.815
	H-2→L (11.6)			2.334	2.351									
S6	H→L+1	no	2.651	2.304	2.380	1.678	1.678	0	2.322	2.328	1.809	1.807	1.808	1.811
				2.367	2.316									
S7	H-1→L+2 (56.0)	yes	2.691	2.295	2.352	1.687	1.686	0.001	2.314	2.355	1.797	1.811	1.790	1.822
	H-4→L+1 (25.2)			2.340	2.423									
S8	H-4→L+1 (72.2)	no	2.652	2.349	2.367	1.684	1.684	0	2.336	2.339	1.794	1.812	1.794	1.815
	H-1→L+2 (16.0)			2.368	2.351									
S9	H→L+2 (35.2)	yes	2.636	2.349	2.385	1.674	1.686	0.012	2.367	2.336	1.810	1.826	1.780	1.793
	H-4→L (20.2) H-1→L+1 (20.0)			2.353	2.361									
S10	H-5→L (48.5)	no	2.661	2.358	2.342	1.683	1.676	0.007	2.339	2.352	1.805	1.802	1.815	1.811
	H-2→L+1 (19.5)			2.352	2.366									
S11	H-2→L+1 (56.1)	no	2.671	2.352	2.354	1.689	1.689	0	2.354	2.35	1.780	1.812	1.792	1.812
	H-1→L+2 (24.9)			2.385	2.386									

[a] Δμ is the difference between the longer and the shorter Fe−H distance. Whenever the geometry optimization did not converge to a stationary point ("no" in the conv column) the geometry parameters are reported for the lowest energy/lowest gradient structure obtained during the same optimization calculation.

dx.doi.org/10.1021/ic400818t | Inorg. Chem. 2013, 52, 9826−9841

Table 8. $2^{+}_{trans\text{-}cis}$ TDDFT Optimized Geometry Parameters (Distances in Å, Angles in Degrees)[a]

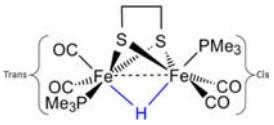

				Fe−S		Fe−H		Δμ	Fe−P		Fe−C			
	1e	conv	Fe−Fe	trans	cis	trans	cis		trans	cis	trans		cis	
GS			2.594	2.307	2.302	1.668	1.669	0.001	2.273	2.268	1.771	1.776	1.778	1.775
				2.302	2.298									
S1	H→L	yes	2.632	2.315	2.366	1.667	1.665	0.002	2.389	2.302	1.842	1.780	1.766	1.782
				2.327	2.327									
S2	H→L(53.4)	no	2.752	2.309	2.319	1.740	1.622	0.118	2.375	2.307	1.832	1.773	1.801	1.771
	H-1→L (45.2)			2.334	2.393									
S3	H-3→L (82.6)	no	2.703	2.308	2.363	1.726	1.628	0.098	2.407	2.290	1.832	1.811	1.787	1.787
	H-2→L (15.7)			2.323	2.343									
S4	H-1→L (53.5)	no	2.726	2.344	2.380	1.746	1.627	0.119	2.395	2.292	1.828	1.780	1.800	1.815
	H-3→L (39.9)			2.301	2.315									
S5	H→L+1 (48.3)	no	2.690	2.396	2.344	1.688	1.658	0.03	2.307	2.310	1.814	1.799	1.814	1.793
	H-2→L (21.4)			2.383	2.318									
S6	H-1→L+1 (56.1)	no	2.673	2.491	2.320	1.663	1.662	0.001	2.286	2.317	1.830	1.800	1.811	1.790
	H-2→L (31.5)			2.360	2.333									
S7	H→L+3 (54.2)	no	2.639	2.386	2.371	1.669	1.666	0.003	2.279	2.359	1.800	1.792	1.845	1.791
	H-1→L+2 (23.7)			2.376	2.394									
S8	H-1→L+2 (32.7)	yes	2.680	2.363	2.375	1.679	1.659	0.02	2.294	2.344	1.821	1.792	1.833	1.792
	H-4→L (30.8)			2.365	2.386									
S9	H-4→L (42.4)	no	2.638	2.331	2.374	1.661	1.664	0.003	2.314	2.330	1.815	1.805	1.817	1.809
	H→L+2 (27.5)			2.404	2.356									
S10	H-1→L+2 (51.5)	no	2.644	2.348	2.366	1.665	1.671	0.006	2.336	2.315	1.798	1.836	1.799	1.832
	H→L+3 (29.0)			2.382	2.340									
S11	H-3→L+1 (36.7)	no	2.676	2.409	2.353	1.671	1.678	0.007	2.311	2.306	1.793	1.837	1.801	1.814
	H-4→L+1 (18.9)			2.356	2.353									

[a] Δμ is the difference between the longer and the shorter Fe−H distance. Whenever the geometry optimization did not converge to a stationary point ("no" in the conv column) the geometry parameters are reported for the lowest energy/lowest gradient structure obtained during the same optimization calculation.

contribution from the other Fe atom. This effect is clearly due to the higher molecular symmetry of $2^{+}_{trans-trans}$ relative to $2^{+}_{trans-cis}$, and it will impact on the nuclear distortion evaluated within geometry optimization. At variance with 1^{+}, no significant CT from or toward the PMe_3 ligand is observed in line with the nature of the FMOs. Finally none of the states considered involve the bridging hydride.

In Table 7 and 8 are reported the main structural parameters obtained by optimizing the excited state structures starting from the trans−trans and trans−cis ground state minima. As already underlined above, when optimization convergence criteria are not met, the parameters associated with structures featuring the lowest energy/gradient norm vector are reported. On average the nuclear distortion observed for the two isomers are similar. In line with the results reported in Table 4 for 1^{+}, all the Fe-L distances result elongated, in particular the Fe−Fe and Fe−S distances. The largest nuclear distortions are observed for the optimized structure of the $2^{+}_{trans-cis}$ isomer. The structures obtained for the S2 and S4 states are characterized by a significant Fe-μH-Fe distortion (Δμ values equal to 0.118 and 0.119 Å, respectively, while it is only 0.001 Å for the ground state structures). At the optimized geometry, these two states are both characterized by the population of the LUMO with a Fe→Fe CT toward the iron atom that binds the PMe_3 in apical position. The optimized S6 structure is characterized by a 0.184 Å elongation of one Fe−S bond with a Fe→Fe CT similar to that observed for S2 and S4.

CONCLUSION

In this contribution, we have investigated the excited state properties of the protonated $Fe^{I}Fe^{I}$ model $[Fe_2(edt)(\mu H)(CO)_4(dppv)]^{+}$ (1^{+}) and $[Fe_2(edt)(\mu\text{-}H)(CO)_4(PMe_3)_2]^{+}$ (2^{+}) using DFT and TDDFT techniques, with the objective of better understanding their photoreactivity in the light of the recent experiments that disclosed their catalytic properties associated with the H_2 evolution reaction *without sensitizer*.[13]

To address such issue, we computed the electronic spectrum of 1^{+} and explored its excited state PES using two approaches, that is, excited PES scan along the Fe-ligand stretching coordinates and full TDDFT geometry optimization.

Simulation of the first instants of the photodynamic process show results depending on which excited state is populated. When considering 1^{+} the lower-energy excited states (S1−S4) are characterized by population of the LUMO and display a Fe_{dppv}→$Fe_{(CO)3}$ MMCT and Fe_{dppv}→(S,CO) MLCT character. Moreover, the Fe−S bond cleavage and the loss of the hydride bridging coordination are favored upon light irradiation, whereas CO photodissociation appears less favored. The TDDFT optimized structure of S1 evidence a Fe−S bond elongation of 0.422 Å which suggests the formation of a transient 5-coordinate species that, from one side, might favor

dx.doi.org/10.1021/ic400818t | Inorg. Chem. 2013, 52, 9826−9841

the migration of the bridging hydride to terminal position, or from the other side, is likely to be readily protonated at the S site. The TDDFT analysis of higher energy states (S6, S8, and S10 in particular) evidences a significant loss of the bridging character of the hydride coordination mode. The same three excited states originate from a π density migration from the phenyl rings of the dppv ligand to the Fe atoms and therefore display a dppv→Fe LMCT character. The loss of bridging character in favor of more terminal character is consistent with higher susceptibility of protonation.[20−22]

The breaking of symmetry affecting the Fe-μH-Fe moiety of $\mathbf{1}^+$ and $\mathbf{2}^+$ along with the Fe−S elongation, are both relatable to higher conformational mobility achieved by the system upon light irradiation. As aforementioned, such two events could trigger a rearrangement process *which is prohibitive at the ground state*, that is, the isomerization leading from μ-hydride to terminal hydride. Our calculations estimate a barrier of only 16 kcal/mol to obtain a terminal hydride on the excited state PES. This is relevant in HER since the former show less or no reactivity toward protons whereas the latter are readily protonated. Unfortunately, the absence of lifetime data of the excited state does not allow one to draw definitive conclusions about the actual accessibility of the photoisomerization.

Nonetheless it may be interesting to underscore that DFT predicts the rearrangement process to be significantly favored at the excited state level vs the ground state one.

The comparison of the results for $\mathbf{1}^+$ and $\mathbf{2}^+$ compounds is important to better understand their electronic structure. Excited state properties of $\mathbf{2}^+$ depend on the isomer considered and, from the HER point of view, TDDFT geometry optimizations suggest that the $\mathbf{2}^+_{\mathrm{trans-cis}}$ isomer should be more reactive. The main difference in the excited state properties of the two compounds is the dppv→Fe CT, which is peculiar of $\mathbf{1}^+$. The comparison among the various geometry optimized excited state structures show that the nuclear distortions observed for $\mathbf{2}^+$ are roughly halved with respect to $\mathbf{1}^+$ (largest Fe−S elongation: 0.422 Å for S1 of $\mathbf{1}^+$; 0.184 Å for S6 of $\mathbf{2}^+_{\mathrm{trans-cis}}$; largest $\Delta\mu$ values; 0.422 Å for S6 of $\mathbf{1}^+$; 0.118 Å for S4 of $\mathbf{2}^+_{\mathrm{trans-cis}}$). It is not straightforward to understand whether the observed differences are enough to assert that $\mathbf{1}^+$ and $\mathbf{2}^+$ could have a different photoreactivity. By inspecting the excited state properties going from the less symmetric $\mathbf{1}^+$ to the more symmetric $\mathbf{2}^+_{\mathrm{trans-trans}}$, we observe a decrease of CT that evidently influences the values of the nuclear distortions of the optimized structures. However, at this level we observed the same type of nuclear distortion (Fe−S bond elongation and losing of hydride bridging character) with only different magnitudes suggesting a common photoreactivity toward HER for $\mathbf{1}^+$ and $\mathbf{2}^+$.

DFT has put in evidence the viability of both protonation pathways of the two hydrides: (i) immediate protonation of the "quasi-terminal" hydride which is generated upon LUMO population; (ii) *if lifetime were to be long enough*, a relatively facile rearrangement toward a fully terminal coordinated isomer (**3b**, Figure 6) and finally decay to the ground state. Such rearrangement could also be favored by the Fe−S bond cleavage with the formation of a transient 5-coordinate species which could evolve toward a terminal hydride structure. However, it is more conceivable that the Fe−S bond cleavage upon excitation leads to another possible scenario: after decay of the excited state, the S ligand, made more basic by the detachment from Fe, could be easily protonated to form a species simultaneously bearing Fe−H and S−H, that is a proper feature to give facile HER. DFT has shown that this route is energetically accessible, at least thermodynamically. Because of the values of the computed redox potentials, no distinction can be made about the actual intimate mechanism of H_2 release by such doubly protonated species. As aforementioned, such last scenario implies strong resemblance between the effect of the photoactivation and the effect of super-reduction of di-Fe(I) dithiolates to Fe(I)Fe(0) species, encountered during electrocatalyzed HER. To the best of our knowledge, none among the three scenarios presented was previously proposed to be associated with diiron carbonyl photoreactivity, usually reported to depend on CO loss.

■ ASSOCIATED CONTENT

Supporting Information

Detailed description of ground state vs photoisomerization (modeled as electronic triplet) pathways of μ-H migration to terminal-H. Cartesian coordinates of selected ground state and excited state geometry optimized structures (coordinates in atomic units). This material is available free of charge via the Internet at http://pubs.acs.org.

■ AUTHOR INFORMATION

Corresponding Author

*E-mail: giuseppe.zampella@unimib.it.

Notes

The authors declare no competing financial interest.

■ REFERENCES

(1) Lomoth, R.; Ott, S. *Dalton Trans.* **2009**, 9952−9959.
(2) Wang, M.; Chen, L.; Li, C.; Sun, L. *Dalton Trans.* **2011**, *40*, 12793−12800.
(3) Ekström, J.; Abrahamsson, M.; Olson, C.; Bergquist, J.; Kaynak, F. B.; Eriksson, L.; Sun, L.; Becker, H-C; Åkermark, B.; Hammarström, L.; Ott, S. *Dalton Trans.* **2006**, *38*, 4599−4606.
(4) Wolpher, H.; Borgström, M.; Hammarström, L.; Bergquist, J.; Sundström, V.; Stenbjörn, S.; Sun, L.; Åkermark, B. *Inorg. Chem. Commun.* **2003**, *6*, 989−991.
(5) Wang, H.; Si, G.; Cao, W.; Wang, W.; Li, Z.; Wang, F.; Tung, C.; Wu, L.-Z. *Chem. Commun.* **2011**, *47*, 8406−8408.
(6) Wang, F.; Wang, W.-G.; Wang, H.; Si, G.; Tung, C.-H.; Wu, L. Z. *ACS Catal.* **2012**, *2*, 407−416.
(7) Streich, D.; Astuti, Y.; Orlandi, M.; Schwartz, L.; Lomoth, R.; Hammarström, L.; Ott, S. *Chem.—Eur. J.* **2010**, *16*, 60−63.
(8) Wang, W.; Wang, F.; Wang, H.; Tung, C.; Wu, L. *Dalton Trans.* **2012**, *41*, 2420−2426.
(9) Cao, W.; Wang, F.; Wang, H.; Chen, B.; Feng, K.; Tung, C.; Wu, L. *Chem. Commun.* **2012**, *48*, 8081−8083.
(10) Na, Y.; Pan, J.; Wang, M.; Sun, L. *Inorg. Chem* **2007**, *46*, 3813−3815.
(11) Na, Y.; Wang, M.; Pan, J.; Zhang, P.; Åkermark, B.; Sun, L. *Inorg. Chem.* **2008**, *47*, 2805−2810.
(12) Zhang, P.; Wang, M.; Na, Y.; Li, X. M.; Jiang, Y.; Sun, L. *Dalton Trans.* **2010**, *39*, 1204−1206.
(13) Wang, W.; Rauchfuss, T. B.; Bertini, L.; Zampella, G. *J. Am. Chem. Soc.* **2012**, *134*, 4525−4528.
(14) Wright, J. A.; Pickett, C. J. *Chem. Commun.* **2009**, *48*, 5719−5721.
(15) Liu, C.; Peck, J. N. T.; Wright, J. A.; Pickett, C. J.; Hall, M. B. *Eur. J. Inorg. Chem.* **2011**, 1080−1093.
(16) Bitterwolf, T. E. *J. Organomet. Chem.* **2004**, *689*, 3939−3952.
(17) Ridley, A. R.; Stewart, A. I.; Adamczyk, K.; Ghosh, H. N.; Kerkeni, B.; Guo, Z. X.; Nibbering, E. T. J.; Pickett, C. J.; Hunt, N. T. *Inorg. Chem.* **2008**, *47*, 7453−7455.

(18) Stewart, A. I.; Wright, J. A.; Greetham, G. M.; Kaziannis, S.; Santabarbara, S.; Towrie, M.; Parker, A. W.; Pickett, C. J.; Hunt, N. T. *Inorg. Chem.* **2010**, *49*, 9563−9573.
(19) Kaziannis, S.; Santabarbara, S.; Wright, J. A.; Greetham, G. M.; Towrie, M.; Parker, A. W.; Pickett, C. J.; Hunt, N. T. *J. Phys. Chem. B* **2010**, *144*, 15370−15379.
(20) Marhenke, J.; Pierri, A. E.; Lomotan, M.; Damon, P. L.; Ford, P. C.; Works, C. *Inorg. Chem.* **2011**, *50*, 11850−11852.
(21) Bertini, L.; Greco, C.; De Gioia, L.; Fantucci, P. *J. Phys. Chem. A* **2009**, *113*, 5657−5670.
(22) Barton, B. E.; Rauchfuss, T. B. *Inorg. Chem.* **2008**, *47*, 2261−2263.
(23) van der Vlugt, J. I.; Rauchfuss, T. B.; Whaley, C. M.; Wilson, S. R. *J. Am. Chem. Soc.* **2005**, *127*, 16012−16013.
(24) Galinato, M. G. I.; Whaley, C. M.; Roberts, D.; Wang, P.; Lehnert, N. *Eur. J. Inorg. Chem.* **2011**, 1147−1154.
(25) Kania, R.; Frederix, P. W. J. M.; Wright, J. A.; Ulijn, R. V.; Pickett, C. J.; Hunt, N. T. *J. Chem. Phys.* **2012**, *136*, 044521.
(26) Becke, A. D. *Phys. Rev. A* **1988**, *38*, 3098−3100.
(27) Perdew, J. P. *Phys. Rev. B* **1986**, *33*, 8822−8824.
(28) Eichkorn, K.; Weigend, F.; Treutler, O.; Ahlrichs, R. *Theor. Chem. Acc.* **1997**, *97*, 119−124.
(29) Ahlrichs, R.; Bar, M.; Haser, M.; Horn, H.; Kolmel, C. *Chem. Phys. Lett.* **1989**, *62*, 165−169.
(30) Schafer, A.; Huber, C.; Ahlrichs, R. *J. Chem. Phys.* **1994**, *100*, 5829−5835.
(31) Furche, F.; Ahlrichs, R. *J. Chem. Phys.* **2002**, *117*, 7433−7447.
(32) Rappoport, D.; Furche, F. *J. Chem. Phys.* **2005**, *122*, 064105.
(33) Fiedler, A. T.; Brunold, T. C. *Inorg. Chem.* **2005**, *44*, 1794−1809.
(34) Georgakaki, I. P.; Thomson, L. M.; Lyon, E. J.; Hall, M. B.; Darensbourg, M. Y. *Coord. Chem. Rev.* **2003**, *238*−*239*, 255−266.
(35) Borg, S. J.; Behrsing, T.; Best, S. P.; Razavet, M.; Liu, X.; Pickett, C. J. *J. Am. Chem. Soc.* **2004**, *126*, 16988−16999.
(36) de Carcer, A. I.; Di Pasquale, A.; Rheingold, A. L.; Heinekey, D. M. *Inorg. Chem.* **2006**, *45*, 8000−8002.
(37) These energy differences were computed taking into account the state crossing found for the lower energy state (S3/S4 for equatorial and apical CO; S1/S2 and S3/S4 for the CO on the dppv side).
(38) Surface scans have been made up on the basis of pathways computed on the ground state surface, which are an approximation of the true relaxation pathways on the excited PES that get worse as one moves away from the ground state minimum structure.
(39) Cohen, R.; Weitz, E.; Martin, J. M. L.; Ratner, M. A. *Organometallics* **2004**, *23*, 23152325.
(40) Zampella, G.; Fantucci, P.; De Gioia, L. *Chem. Commun.* **2010**, *46*, 8824−8826.
(41) Zampella, G.; Fantucci, P.; De Gioia, L. *J. Am. Chem. Soc.* **2009**, *131*, 10909−10917.
(42) Tschierlei, S.; Ott, S.; Lomoth, R. *Energy Environ. Sci.* **2011**, *4*, 2340−2352.
(43) Ezzaher, S.; Capon, J.-F.; Gloaguen, F.; Petillon, F. Y.; Schollhammer, P.; Talarmin, J. *Inorg. Chem.* **2007**, *46*, 3426−3428.
(44) Barton, B. E.; Zampella, G.; Justice, A. K.; De Gioia, L.; Rauchfuss, T. B.; Wilson, S. R. *Dalton Trans.* **2010**, *39* (12), 3011−3019.
(45) Olsen, M. T.; Gray, D. L.; Rauchfuss, T. B.; De Gioia, L.; Zampella, G. *Chem. Commun.* **2011**, *47*, 6554−6556.
(46) Greco, C.; Zampella, G.; Bertini, L.; Bruschi, M.; Fantucci, P.; De Gioia, L. *Inorg. Chem.* **2007**, *46*, 108−116.
(47) Felton, G.A. N.; Vannucci, A. K.; Chen, J.; Lockett, L. T.; Okumura, N.; Petro, B. J.; Zakai, U. I.; Evans, D. H.; Glass, R. S.; Lichtenberger, D. L. *J. Am. Chem. Soc.* **2007**, *129*, 12521−12530.
(48) Greco, C.; Fantucci, P.; De Gioia, L.; Suarez-Bertoa, R.; Bruschi, M.; Talarmin, J.; Schollhammer, P. *Dalton Trans.* **2010**, *39* (31), 7320−7329.
(49) Liedel, N.; Hsieh, C.-H.; Chernev, P.; Sigfridsson, K. G. V.; Darensbourg, M. Y.; Haumann, M. *Dalton Trans.* **2013**, *42*, 7539−7554.